Low-Temperature Processing of ZrB_2-ZrC Composites by Reactive Hot Pressing

LINGAPPA RANGARAJ, SIRIYARA J. SURESHA, CANCHI DIVAKAR, and VIKRAM JAYARAM

Dense ZrB_2-ZrC and ZrB_2-$ZrC_{x\sim0.67}$ composites have been produced by reactive hot pressing (RHP) of stoichiometric and nonstoichiometric mixtures of Zr and B_4C powders at 40 MPa and temperatures up to 1600 °C for 30 minutes. The role of Ni addition on reaction kinetics and densification of the composites has been studied. Composites of ~97 pct relative density (RD) have been produced with the stoichiometric mixture at 1600 °C, while the composite with ~99 pct RD has been obtained with excess Zr at 1200 °C, suggesting the formation of carbon deficient ZrC_x that significantly aids densification by plastic flow and vacancy diffusion mechanism. Stoichiometric and nonstoichiometric composites have a hardness of ~20 GPa. The grain sizes of ZrB_2 and $ZrC_{x\sim0.67}$ are ~0.6 and 0.4 μm, respectively, which are finer than those reported in the literature.

DOI: 10.1007/s11661-008-9500-y

I. INTRODUCTION

REFRACTORY transition metal borides and carbides, such as ZrB_2, ZrC, HfB_2, HfC, and TaC, have been called ultra-high-temperature ceramics (UHTCs), because of their high melting points (> 3000 °C), better oxidation and corrosion resistance. The UHTCs have been investigated for applications that include thermal protection materials for advanced re-entry vehicles, molten metal crucibles, and high-temperature electrodes.[1–3] The high melting point, strong covalent bonding and low self-diffusion coefficient of ZrB_2-based composites typically require pressure-assisted sintering at very high temperatures (> 1900 °C). The $ZrC_{0.9}$-ZrB_2 composite has been produced by sintering and directional solidification in argon atmosphere at 2300 °C.[4,5] The hardness and fracture toughness of the composites were 24 GPa and 5.44 MPa$\sqrt{m}$, respectively. Composites of ZrB_2-ZrC have been fabricated by infiltration of Zr metal into the B_4C preform at 1850 °C to 2000 °C for 1 to 2 hours.[6–10] These composites showed the formation of ZrB_2-ZrC_x with free Zr metal. The self-propagating high-temperature synthesis of mechanically alloyed Zr-B-C powder (MA-SHS) was used to produce the ZrB_2-ZrC powder composite in air followed by spark plasma sintering (SPS). The relative density (RD), hardness and fracture toughness were 98 pct, 17.8 GPa, and 3.4 MPa$\sqrt{m}$, respectively.[11–12] High-density ZrB_2-based materials have also been obtained by hot pressing at temperatures lower than 2000 °C with the addition of sintering aids such as Ni[13] and pressureless sintering at temperature ~1850 °C with the addition of B_4C.[14] SPS of ZrB_2-ZrC composites with the addition of lanthanum (1 to 5 wt pct) enhanced the RD to 99 pct and reduced the densification temperature to 1800 °C.[15] Reactive hot pressing (RHP) of Zr and B_4C powder mixture at 30 MPa and 1900 °C for 60 minutes resulted in 98.4 pct RD with a bending strength of ~450 MPa.[16] The two-stage transient plastic phase processing of three different molar ratios of Zr to B_4C (3:1, 3.5:1, and 4:1) at a final temperature of 1600 °C for 4 hours yielded ZrB_2-ZrC composites with full density.[17] It has been recently shown that high energy milling of elemental Zr and B can be used to produce ZrB_2 at temperatures as low as 600 °C, and dense ZrB_2-SiC composites can be obtained at 1700 °C.[18]

Because boron compounds are cheaper and easier to handle, the present study is undertaken to systematically establish the possibility of lowering the process temperature by reactive densification of ZrB_2-ZrC composites starting with Zr and B_4C powders. In an earlier work on processing of TiN-TiB_2 composites, it was shown that a small amount of Ni (1 wt pct) addition to the starting Ti-BN mixture could substantially decrease the densification temperature from 1850 °C to 1400 °C.[19] The presence of a transient Ti-Ni liquid phase was shown to aid not only pore removal but also completion of the reaction. Because the eutectic in the Zr-rich portion of the Zr-Ni phase diagram is similar to the Ti-rich portion in Ti-Ni, our aim was to investigate the effect of Ni addition and to examine whether temperatures as high as those commonly used are essential. The effect of excess Zr on reaction kinetics and densification has also been studied.

LINGAPPA RANGARAJ, Scientist "E1", and CANCHI DIVAKAR, Scientist "F", are with the Materials Science Division, National Aerospace Laboratories, Bangalore-560 017, India. SIRIYARA J. SURESHA, Materials Research Centre, and VIKRAM JAYARAM, Professor, Department of Materials Engineering, are with the Indian Institute of Science, Bangalore-560 012, India. Contact e-mail: qjayaram@materials.iisc.ernet.in

This article is based on a presentation given in the symposium entitled "Materials Behavior: Far from Equilibrium" as part of the Golden Jubilee Celebration of Bhabha Atomic Research Centre, which occurred during December 15–16, 2006 in Mumbai, India.

Article published online March 28, 2008

II. EXPERIMENTAL PROCEDURE

The stoichiometric ZrB_2-ZrC and nonstoichiometric ZrB_2-ZrC_x composites were produced by RHP of zirconium (Zr) and boron carbide (B_4C) powders using the following reactions, which have large negative free energies:[16]

$$3Zr + B_4C \rightarrow 2ZrB_2 + ZrC \quad [1]$$

$$3.5Zr + B_4C \rightarrow 2ZrB_2 + 1.5ZrC_{\sim 0.67} \quad [2]$$

The expected volume fractions of the individual phases formed from Reaction [1] are 70.38 pct ZrB_2 and 29.62 pct ZrC and from Reaction [2] are 61.64 pct ZrB_2 and 38.36 pct $ZrC_{\sim 0.67}$. The theoretical densities of the composites with 1 wt pct Ni, according to the rule of mixtures, are 6.31 and 6.26 g/cm^3, respectively. Density values of 6.1 g/cm^3 for ZrB_2, 6.73 g/cm^3 for ZrC, and 6.47 g/cm^3 for $ZrC_{\sim 0.67}$ are used in the calculation of the theoretical density of the composites.

A. *Materials and Processing*

Commercial powders of Zr: purity ~98 pct, particle size 2 to 10 μm (M/s Yashoda Special Metals, Hyderabad, India); B_4C: purity ~99 pct, particle size 10 to 20 μm; D_{50}: 11 μm (M/s Boron Carbide India Ltd., Mumbai); and Ni: purity ~99.5 pct, particle size ~4 μm (M/s Inco, London, UK) have been used in the present study. The analysis report supplied by the manufacturer indicates B + C: > 99 pct, free carbon < 1 pct; Fe: < 0.2 pct; B_2O_3: < 0.4 pct; and Si: < 0.091 pct for the B_4C powder. X-ray diffraction (XRD) patterns of the starting B_4C and Zr powders are given in Figure 1, and B_4C powder indicated a small carbon (graphite) peak (Figure 1(a)).

The required amounts of Zr and B_4C powders were mixed in ethanol using ZrO_2 (8 mol pct Y_2O_3) milling media for 24 hours in a plastic bottle and dried at ~100 °C. Powder mixtures with 1 wt pct Ni were also prepared. The weight loss of the milling media measured after each mixing is ~2 wt pct, indicating ZrO_2 may be present as impurity in the starting mixture. The dried powder mixtures were filled in a graphite die (25-mm internal diameter and 80-mm height). Direct contact between the powder mixture and die/punch assembly was avoided by using flexible graphite sheet (0.2-mm thickness). The RHP experiments were conducted in a vacuum hot press (Materials Research Furnaces, Suncook, NH). A typical RHP experiment involved the following steps: after evacuating the furnace to 5×10^{-5} torr, the samples were heated to 300 °C at 4 °C/min, held for 15 minutes to remove the gases present on the surface of the particles, and heated at 5 °C to 10 °C/min to different required temperatures and maintained for 30 minutes. The pressure of 40 MPa on the sample was usually applied ~25 minutes before reaching the final temperature, held for the required time, and released within 10 minutes from the start of the cooling sequence. The sample assembly was cooled to room temperature at 10 °C/min.

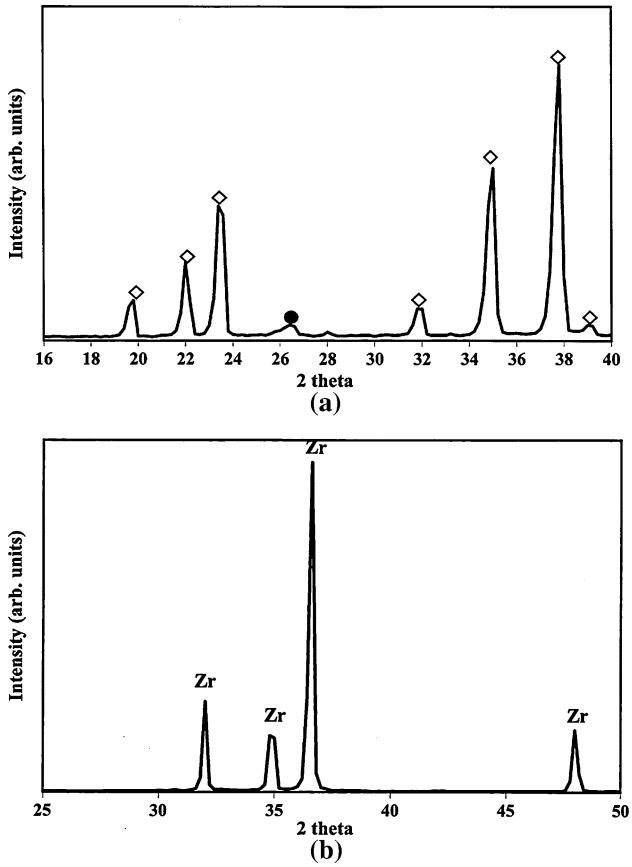

Fig. 1—XRD patterns of the starting powders: (*a*) B_4C (◇—B_4C and ●—graphite) and (*b*) Zr. The starting B_4C powder shows a small graphite impurity peak.

The RHP experiments with stoichiometric mixtures were conducted in the temperature range 1200 °C to 1600 °C for 30 minutes. In the experiments up to 1400 °C, the application of pressure was initiated at 1000 °C and the pressure was maintained for 30 minutes. For the experiment at 1600 °C, the application of pressure was initiated at 1200 °C. The RHP experiments with nonstoichiometric mixture were conducted in the temperature range 1000 °C to 1400 °C for 5 to 30 minutes.

B. *Characterization of Reactive Hot-Pressed Composites*

The top and bottom surfaces of reactively hot-pressed composites were ground and polished using SiC abrasive paper and diamond paste down to 0.25 μm using an automatic polishing machine (Ecomet 4000 with Automet 2000, M/s Buehler, Lake Bluff, Illinois) followed by ultrasonic cleaning with acetone. The XRD patterns were recorded (Philips, Eindhoven, The Netherlands) using Cu K_α radiation to identify the phases present in the composites. The lattice parameter (Å) of ZrC in stoichiometric and nonstoichiometric composites was calculated by recording the XRD patterns in the 2θ range of 94 to 154 deg (using graphite monochromator in the diffracted beam) and using standard extrapolation functions to determine the true lattice parameter at a Bragg angle of 90 deg. Density measurements were

conducted using the water displacement method after boiling the samples in water for 1 hour and cooling to room temperature. Vickers hardness measurements (Model HSV-20, Shimadzu Corporation, Kyoto, Japan) were performed on the polished surfaces at a test load of 500 g (4.9 N) and a holding period of 15 seconds. An average of 15 readings was taken for each reported value. Microstructural observations of polished surfaces were made using optical microscopy (Axiovert 200 M MAT, Carl Zeiss Light Microscopy, Goettingen, Germany), scanning electron microscopy (SEM) (FEI-Sirion, Eindhoven, The Netherlands) with energy-dispersive X-ray microanalysis (EDAX, super-ultra-thin window, Genesis Spectrum, Mahwah, NJ), and transmission electron microscopy (TEM) (FEI Tecnai F30, Eindhoven, The Netherlands) along with EDAX at 300 kV operating voltage. The average grain size of ZrB_2 and ZrC reported has been measured through image analysis of the SEM micrographs by the line intercept method by counting a minimum of 300 grains. The selected polished samples were etched using $HF:HNO_3:H_2O$ solution in the ratio of 2:3:95 for 10 seconds.[10] The amount of unreacted B_4C present in the composite was also estimated using optical micrographs. The TEM samples were prepared through conventional specimen preparation steps of dimpling and argon ion beam milling.

III. RESULTS

Initially, the results on the stoichiometric ZrB_2-ZrC composite produced with and without nickel addition in the temperature range 1200 °C to 1600 °C are presented. The role of excess Zr on the reaction and densification of the composite at lower temperatures in the temperature range 1000 °C to 1400 °C is presented later. The experimental conditions, phases observed, density, and hardness of the stoichiometric and nonstoichiometric composites are presented in Tables I and II.

A. *Stoichiometric ZrB_2-ZrC Composites*

The XRD patterns of the polished surfaces of the ZrB_2-ZrC composites produced at 40 MPa, 1200 °C for 30 minutes with 1 wt pct Ni and without Ni are shown in Figure 2. The patterns show only ZrB_2 and ZrC phases with a small peak of ZrO_2; lines corresponding to the starting Zr and B_4C are not present in any of the composites. The measured lattice parameter of the ZrC in the composite produced with Ni is 4.686 ± 0.001 Å and does not change with processing temperature (1200 °C to 1600 °C). The measured lattice parameter without Ni is also 4.686 ± 0.001 Å at 1600 °C. Typical optical micrographs of the composites produced at 40 MPa, 1200 °C for 30 minutes with 1 wt pct Ni and without Ni are shown in Figure 3. The RD of the composites is calculated using the measured bulk density and theoretical density of sample calculated using the rule of mixtures, as predicted by the reaction stoichiometry. The density of the composite (with or without Ni) increases from 5.428 g/cm^3 (86 pct RD) at 1200 °C to 6.131 g/cm^3 (97.2 pct RD) at 1600 °C (Table I). It appears that there is no effect of Ni addition on densification. However, the composite produced at 1200 °C with Ni does not show unreacted B_4C particles

Table I. Experimental Conditions, Density, Phases Observed, and Hardness of the Stoichiometric ZrB_2-ZrC Composites

Sl No.	Experimental Conditions (MPa/°C/Min)	Bulk Density, g/cm^3 (RD)	Phases Present	Hardness (GPa)
1	40/1200/30 (1 wt pct Ni)	5.428 ± 0.024 (86.1 pct)	ZrB_2, ZrC	—
2	40/1200/30	5.443 ± 0.009	ZrB_2, ZrC, B_4C^* (2.97 pct)	—
3	40/1400/30 (1 wt pct Ni)	6.058 ± 0.003 (96.1 pct)	ZrB_2, ZrC	18.9 ± 0.8
4	40/1400/12	5.966 ± 0.004 (95 pct)	ZrB_2, ZrC	—
5	40/1600/30 (1 wt pct Ni)	6.131 ± 0.003 (97.2 pct)	ZrB_2, ZrC	21.1 ± 1.1
6	40/1600/30	6.110 ± 0.003 (97.2 pct)	ZrB_2, ZrC,	20.1 ± 1.8

*Observed by optical microscopy and SEM.

Table II. Experimental Conditions, Density, Phases Observed, and Hardness of the Nonstoichiometric ZrB_2-ZrC Composites

Sl No.	Experimental Conditions (MPa/°C/min)	Bulk Density, g/cm^3 (RD)	Phases Present	Hardness (GPa)
1	–/1000/5 (1 wt pct Ni)	4.299 ± 0.057	ZrB_2, ZrC, Zr, B_4C^{**}	—
2	40/1000/30 (1 wt pct Ni)	5.723 ± 0.009	ZrB_2, ZrC, Zr,* B_4C^{**}	—
3	40/1000/30	5.705 ± 0.003	ZrB_2, ZrC, Zr,* B_4C^{**}	—
4	40/1200/30 (1 wt pct Ni)	6.201 ± 0.008 (99 pct)	ZrB_2, ZrC	22.1 ± 0.7
5	40/1200/30	6.103 ± 0.003	ZrB_2, ZrC, B_4C^{**} (0.28 pct)	19.7 ± 4.5
6	40/1400/30 (1 wt pct Ni)	6.263 ± 0.002 (99.9 pct)	ZrB_2, ZrC	22.4 ± 0.7

*Weak peaks observed in XRD.
**Observed by optical microscopy and SEM.

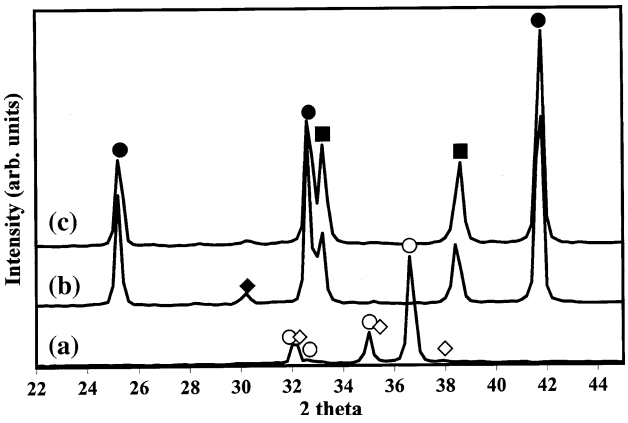

Fig. 2—XRD patterns of the stoichiometric ZrB_2-ZrC composites at 40 MPa, 1200 °C for 30 min: (*a*) starting powder mixture, (*b*) composite with 1 wt pct Ni, and (*c*) composite without Ni (●—ZrB_2, ■—ZrC, ○—Zr, ◇—B_4C, and ♦—ZrO_2). Note that owing to the coverage of B_4C particles by the heavy element zirconium, during mixing, the peaks for B_4C are not visible.

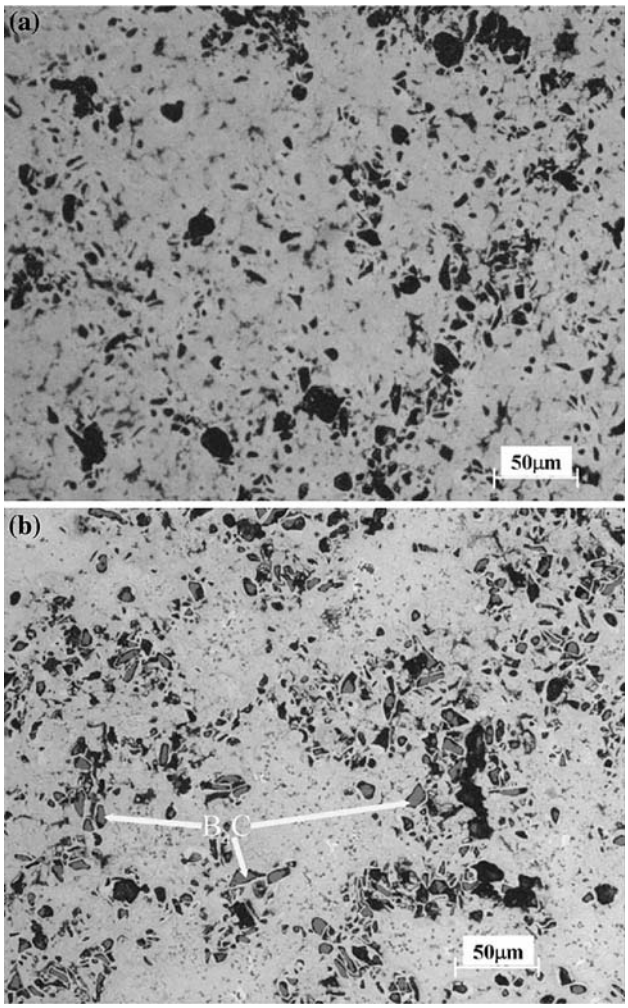

Fig. 3—Optical micrographs of the ZrB_2-ZrC composites produced at 40 MPa, 1200 °C for 30 min: (*a*) with 1 wt pct Ni and (*b*) without Ni. The gray regions are unreacted B_4C particles, as evidenced from the B and C signals in the X-ray spectrum (not shown).

in contrast to ~3 vol pct B_4C estimated in the composite without Ni (Figure 3(b) and Table I), thereby suggesting that Ni aids in the completion of the reaction. Typical SEM micrographs of the etched composite produced at 1400 °C and 1600 °C with Ni are shown in Figures 4(a) and (b). Only a few pores are present without any residual B_4C. The EDAX spectra of the ZrB_2 and ZrC grains are shown in Figures 4(c) and (d). An enlarged view of the spectra shows the ability to resolve the closely spaced Zr, C (inset in Figure 4(d)). The presence of ZrB_2 is indicated by a flattening of the peak due to the overlap of the Zr-M and B-K lines (inset in Figure 4(c)). The grain sizes of ZrB_2 and ZrC phases are 0.65 ± 0.2 μm and 0.44 ± 0.2 μm, respectively, for the composites produced at 1400 °C and 1.56 ± 0.6 μm and 1.15 ± 0.4 μm, respectively, for the composites produced at 1600 °C. These values are significantly lower than 5 to 10 μm for ZrB_2 and 2 to 7 μm for ZrC reported earlier,[10,11,15] but comparable to the submicron sizes of 0.5 ± 0.3 μm reported for ZrB_2 in the ZrB_2-SiC composite.[18] The TEM micrograph of the stoichiometric composite and electron diffractograms of the ZrB_2 and ZrC phases produced at 1400 °C are shown in Figure 5. The TEM-EDAX analyses of the carbide grains show a C/Zr stoichiometry of 65/35 with a scatter of 7 pct.

The hardness of the ZrB_2-ZrC composite produced at 1600 °C for 30 minutes are ~19 to 20 GPa, which is better than 17 GPa for samples produced by SPS.[11,12]

B. *Nonstoichiometric ZrB_2-ZrC_x Composites*

The XRD patterns of nonstoichiometric ZrB_2-ZrC_x composites produced at different temperatures (1000 °C and 1200 °C) are shown in Figure 6. Substantial formation of ZrB_2 and ZrC can be observed just after 5 minutes at 1000 °C (Figure 6(b)). At 1200 °C, the reaction was complete after 30 minutes and the XRD patterns reveal only ZrB_2 and $ZrC_{x\sim0.67}$ phases. The weak reflections that arise from carbon vacancy ordering in $ZrC_{x\sim0.67}$ could not be detected (JCPDS: 32-1489). The measured lattice parameter of nonstoichiometric $ZrC_{x\sim0.67}$ in the composite is 4.682 ± 0.001 Å and also does not change with processing temperature (1200 °C/1400 °C). The TEM micrograph of the nonstoichiometric composites produced at 1400 °C is shown in Figures 7. The electron diffraction patterns confirm the presence of ZrB_2 and ZrC with no evidence for any superlattice reflections from any carbon vacancy ordering. The TEM-EDAX analysis of the carbide grains showed a change in C/Zr stoichiometry to 50:50 in the nonstoichiometric grains with a scatter of 7 pct. Absolute quantitative estimation of carbon by EDAX is unreliable owing to contamination and absorption. However, if we use the composition determined from the stoichiometric composite, which is 65:35, as reported previously, as a 1:1 standard, it is clear that the material made with excess Zr displays the same rock-salt carbide phase with a significant substoichiometry in the carbon content.

The density variations with the processing temperature of nonstoichiometric composites are given in

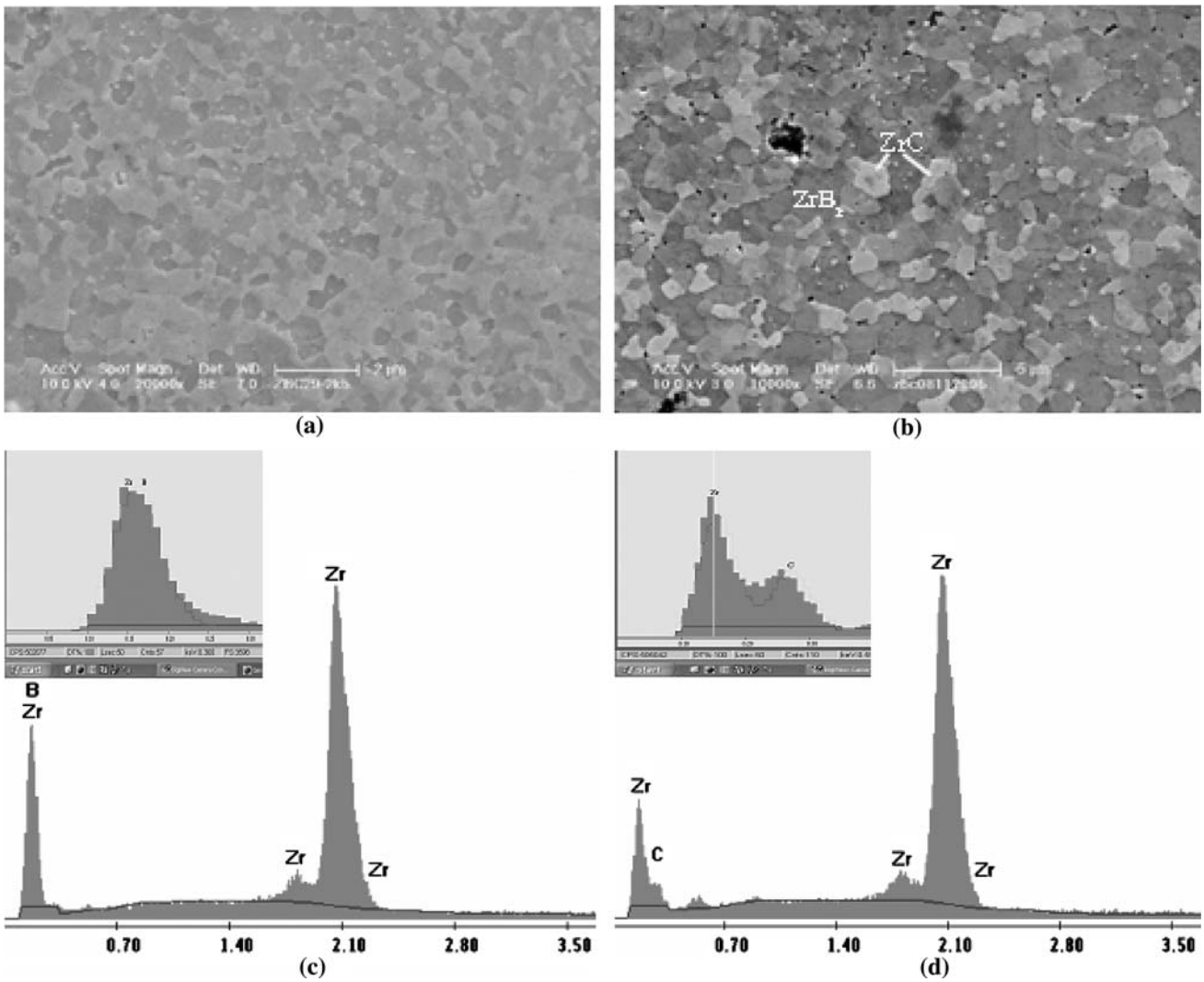

Fig. 4—SEM micrographs of the etched ZrB_2-ZrC composite produced at 40 MPa, for 30 min with 1 wt pct Ni: (*a*) 1400 °C and (*b*) 1600 °C. The dark gray particles are ZrB_2, and the light ones are ZrC particles, as shown by the respective B and C signals in the X-ray spectra in (*c*) and (*d*). Spectra from two principle phases, ZrB_2 and ZrC, are shown in (c) and (d) as insets at a high resolution to show the ability to distinguish the two phases based on the low-energy peaks.

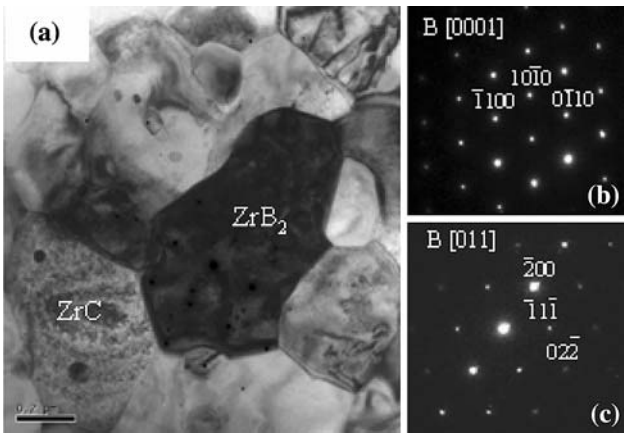

Fig. 5—(*a*) Bright-field TEM micrographs of ZrB_2-ZrC composite produced at 40 MPa, 1400 °C, 30 min (1 wt pct Ni) with selected area electron diffraction patterns for the (b) ZrB_2 and (c) ZrC phases.

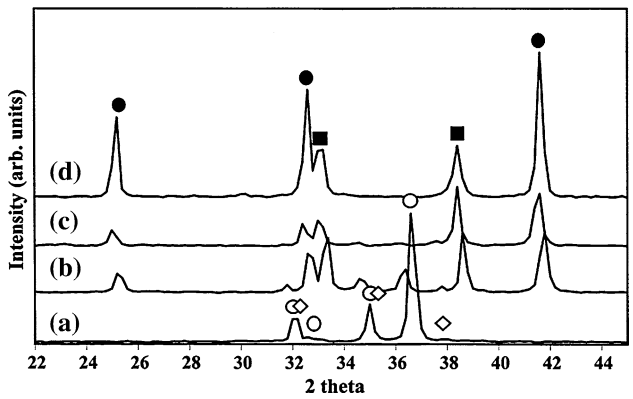

Fig. 6—XRD patterns of the nonstoichiometric ZrB_2-ZrC_x composites produced with 1 wt pct Ni: (*a*) unreacted powder mixture, (*b*) —/1000 °C/5 min, (*c*) 40 MPa/1000 °C/30 min, and (*d*) 40 MPa/1200 °C/30 min (●—ZrB_2, ■—ZrC_x, ○—Zr, and ◇—B_4C).

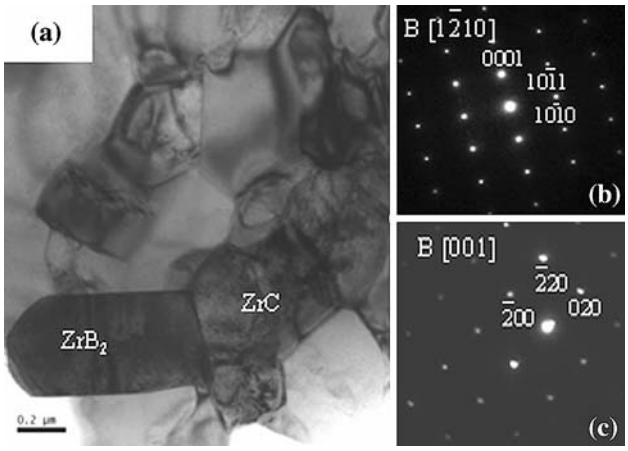

Fig. 7—(*a*) Bright-field TEM micrographs of ZrB_2-$ZrC_{x-0.67}$ composite produced at 40 MPa, 1400 °C for 30 min (1 wt pct Ni) with selected area electron diffraction patterns for the (b) ZrB_2 and (c) ZrC.

Table II. It may be noted that the composite with near theoretical density has been achieved even at 1200 °C. It is also observed that the addition of Ni (1 wt pct) results in an increase of density from 6.1 to 6.2 g/cm^3 (99 pct RD) at 1200 °C. Typical optical micrographs of the composites produced at 40MPa, 1200 °C for 30 minutes without and with 1 wt pct Ni are shown in Figure 8. Unreacted B_4C particles may be seen when Ni is absent (Figure 8(a)), but the composite containing Ni shows completion of the reaction, as seen in the optical micrographs of material made at 1200 °C (Figure 8(b)). Thus, Ni is important to ensure completion of the reaction (Table II).

The early stages of reaction at 1000 °C for 5 minutes are shown in Figure 9. The unreacted B_4C particles and residual metal along with the reaction products are seen (Figure 9(a)) and can be correlated with the XRD observations (Figure 6(b)). The EDAX spectra of the B_4C regions in Figure 9(b) show resolvable B and C K-lines (inset), while regions devoid of B and C, which were identified as metallic in the composite (Figure 9(c)), indicate a semiquantitative composition of 86 at. pct Zr and 14 at. pct Ni. After 30 minutes holding at 1000 °C, the Ni concentration increases to 23 at. pct, illustrating the progress of the reaction. The magnified view of the region around the unreacted B_4C particle (Figure 9(d)) reveals platelet morphology of the ZrB_2/ZrC_x. Typical SEM micrographs of the composites produced at 1200 °C and 1400 °C are shown in Figure 10. The ZrB_2 and $ZrC_{x\sim0.67}$ grains produced are in the submicron range and are 0.64 ± 0.3 μm and 0.43 ± 0.2 μm, respectively (1200 °C). These are somewhat lower than those in the stoichiometric composites produced at 1600 °C in the present study (1.56 ± 0.6 μm for ZrB_2 and 1.15 ± 0.4 μm for ZrC) and much lower than those reported in the literature.[10,15] The hardness of the ZrB_2-$ZrC_{x\sim0.67}$ composite produced at 1200 °C and 30 minutes with Ni is ~22 GPa.

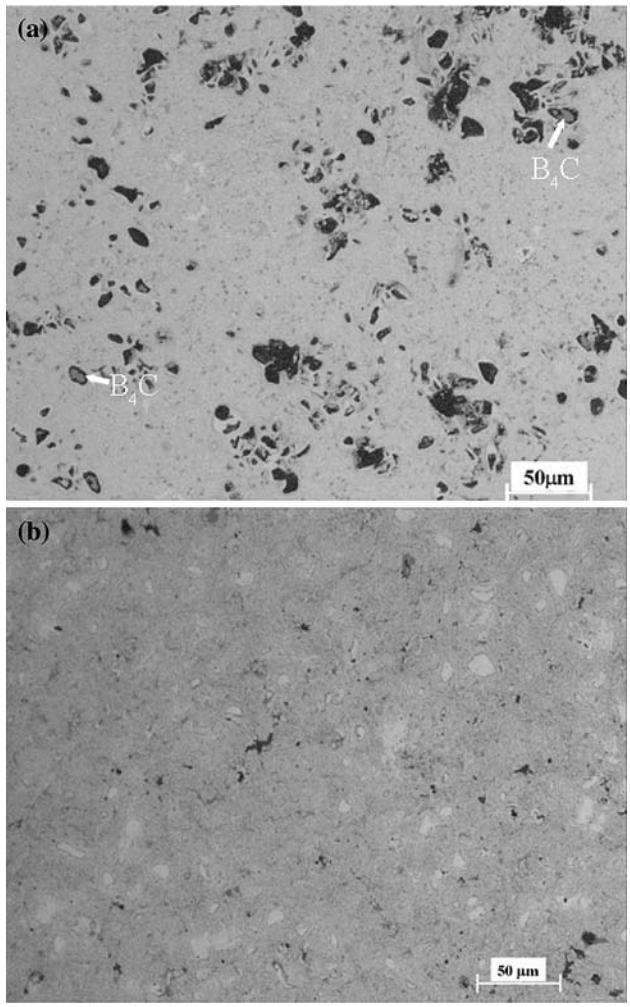

Fig. 8—Optical micrographs of the ZrB_2-$ZrC_{x-0.67}$ composites produced at 40 MPa, 1200 °C for 30 min: (*a*) without Ni showing unreacted B_4C particles and (*b*) with 1 wt pct Ni showing completion of reaction. The dark regions are pores.

IV. DISCUSSION

The principal findings in the results in Section III, *i.e.*, the ability to densify ZrB_2-ZrC composites at temperatures well below 1900 °C and the pronounced role of excess Zr on reaction and densification of the composites, will be examined in turn.

A. *Effect of Processing Temperature on Densification of Stoichiometric Composites*

The reduction in densification temperature for the stoichiometric composite from those in excess of 1900 °C[16] to as low as 1400 °C to 1600 °C suggests that the reaction products are significantly sinterable. One possible reason is the fine scale of the microstructure and the resulting presence of a large number of interfaces (ZrB_2/ZrC; Figure 4) that can aid diffusive transport, similar to that observed in the reaction sintering of TiN-TiB_2 composite[20] and the RHP of ZrB_2-SiC composite,[18] where the TiB_2 and ZrB_2 grains

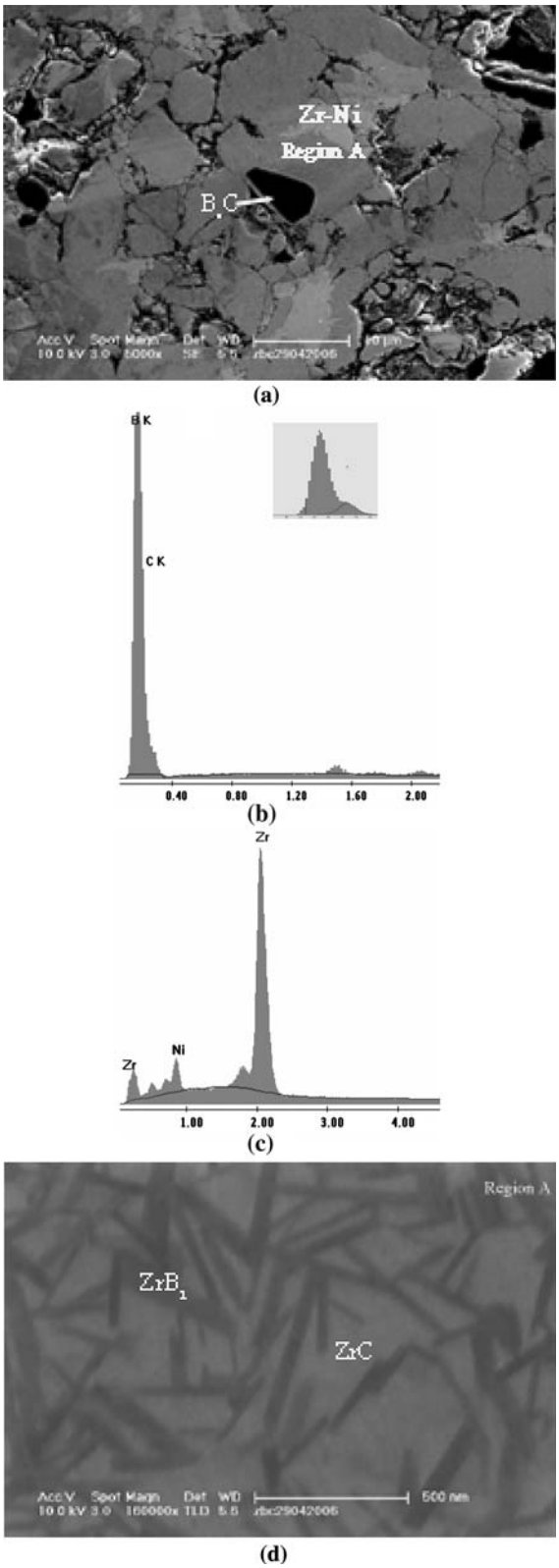

Fig. 9—SEM micrographs of the ZrB_2-ZrC_x composites produced at 1000 °C in 5 min with 1 wt pct Ni: (*a*) unreacted dark grains of B_4C and metallic regions, (*b*) EDAX spectra of B_4C grain, inset shows the separation of B and C, (*c*) EDAX spectra of the metallic region-Zr-Ni (86 at. pct-14 at. pct), and (*d*) region A-ZrB_2 platelets (dark gray) with ZrC.

were also in the submicron range. In the present case, both the ZrB_2 and ZrC grains are finer and the microstructural scale achieved here is significantly lower than those produced earlier in conventional hot pressing/sintering. Because composites with 86 pct RD have been attained even at 1200 °C (Table I), it seems possible that a fine, interpenetrating microstructure with a large number of interfaces prevailed in the crucial, second stage of sintering. The formation of the composite product is by dissociation of B_4C and diffusion of B and C into Zr (Figure 9(a)). Also, the formation of the boride-carbide mixture is accompanied by a volume reduction of ~19 pct, which can lead to cracking and a further refinement of the microstructure due to local crushing under applied pressure.

B. *Effect of Nonstoichiometry on Reaction and Densification of the Composites*

The most remarkable finding is the pronounced role played by excess Zr in reducing the process temperature to achieve full density to 1200 °C—an unprecedented low value in ZrB_2-ZrC composites (Table II). The absence of elemental Zr from XRD (Figure 6(d)) or optical (Figure 8(b))/SEM (Figure 10(a)) micrographs, the high hardness (similar to that of the stoichiometric composite), and the evidence from TEM-EDAX (C/Zr ratio) clearly support the formation of nonstoichiometric zirconium carbide. The differences in the measured lattice parameter for ZrC and $ZrC_{x\sim0.67}$ in the composites (4.686 and 4.682 Å) are consistent with the trends reported in the literature ($ZrC_{0.97}$-4.698 Å and $ZrC_{0.58}$-4.691 Å).[21,33] The formation of platelet morphology (Figure 9(d)) of the ZrB_2/ZrC_x is similar to that seen in melt infiltrated samples containing excess Zr metal[6–10] and those samples produced in two-stage processing.[17] In the present study, it is also noticed that the unreacted B_4C was accompanied by the presence of ZrB_2 platelets from which one may conclude that free Zr also exists. As the reaction progresses, the metal is eliminated with the formation of ZrB_2-$ZrC_{x\sim0.67}$ phases and results in an equiaxed microstructure (Figures 10(a) and (b)). The composite produced without Ni at 1200 °C showed a small amount of unreacted B_4C in the nonstoichiometric composite (0.28 vol pct; Table II), which is significantly lower than in the stoichiometric composite (2.97 vol pct; Table I). This confirms that while Ni can help the reaction, the addition of excess Zr can, by itself, also increase the reaction kinetics. The B_4C contains some free carbon, which may be used to form more ZrC than expected from the reactions, though this change is difficult to notice experimentally. Notice that despite the presence of some free carbon in the starting B_4C, there is no evidence for unreacted graphite in the final stoichiometric composite. It is generally believed that the oxides of B_2O_3 and ZrO_2 on the surface of B_4C and Zr inhibit the densification by promoting coarsening through evaporation condensation at temperatures of 1500 °C to 1800 °C.[22–24] In the present case, it is proposed that any excess carbon in the B_4C would reduce the B_2O_3 or ZrO_2 (from oxidation of Zr or from

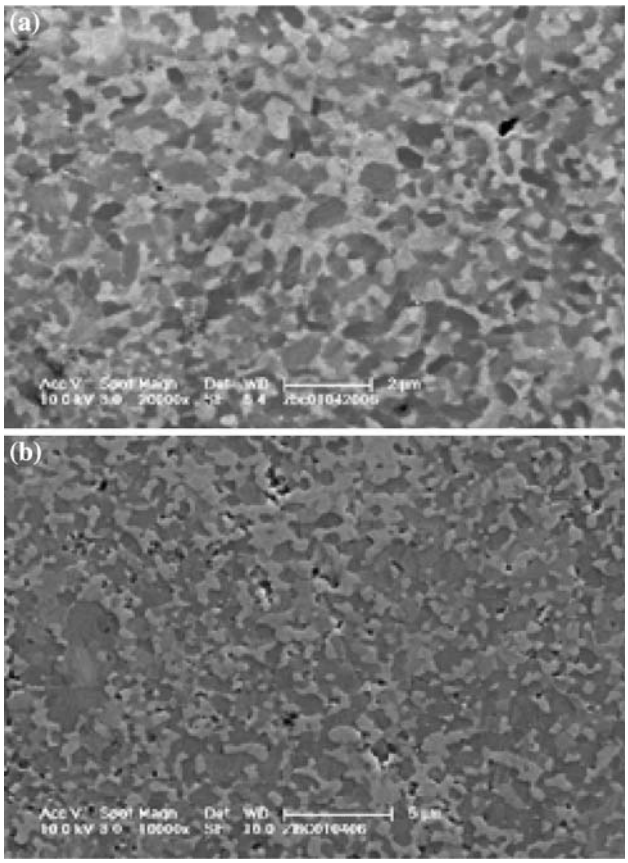

Fig. 10—SEM micrographs of the etched nonstoichiometric ZrB_2-$ZrC_{-0.67}$ composites produced at 40 MPa, 30 min with 1 wt pct Ni: (*a*) 1200 °C and (*b*) 1400 °C. The dark grains are ZrB_2 and the light ones are $ZrC_{x-0.67}$. Both phases display grain sizes in the submicron range.

ZrO_2 milling media) by the following reactions: $2ZrO_2 + B_4C + 3C \rightarrow 2ZrB_2 + 4CO$ (g) and $ZrO_2 + B_2O_3$ (l) $+ 3C \rightarrow ZrB_2 + 3CO$ (g). Recently, it has also been shown that these reactions are thermodynamically favorable at 1000 °C and 1044 °C, respectively, during vacuum sintering.[25] A hint that such a gas evolution might be taking place comes from the observation that the vacuum level suddenly drops around ~900 °C.

We now address the issue of how such a microstructure as described previously can promote densification at low temperature with specific reference to yielding and creep. The transition metal carbides are known to exist over a range of compositions, *e.g.*, Ti, Zr, and Hf carbides have C/metal ratio ranging from 0.65 to 0.98.[21,26,28,29] In this context, the temperature dependence of the yield behavior with respect to nonstoichiometry assumes importance. For example, the yield strength of $TiC_{0.66}$ is about 65 MPa as compared to 450 MPa for $TiC_{0.93}$ at 1200 °C.[26] Also, at temperatures around 1000 °C, the carbides of Ti and Zr undergo brittle-to-ductile transition and deform readily on $\{111\}\langle 1\bar{1}0\rangle$[26–30] in addition to the room-temperature slip system of $\{110\}\langle 1\bar{1}0\rangle$. In reactive densification of the Ti/B_4C system, it has been reported that the formation of TiC_x helps in the densification of TiB_2-TiC composites.[31,32] Also, in the case of $TiC_{0.95}$, the critical resolved shear stress (CRSS) decreased from ~141 to ~72 MPa, and for $TiC_{0.83}$, the CRSS decreased from ~91 MPa at 1000 °C to ~46 MPa at 1200 °C, respectively. ZrC, like its group IV counterpart TiC, shows a falling yield stress with deviations from ideal stoichiometry.[21,28] For $ZrC_{0.875}$, the CRSS reduces from ~163 MPa at 1000 °C to ~87 MPa at 1200 °C.[28] The present composite has a likely stoichiometry of $ZrC_{x\sim0.67}$ and hence its CRSS is expected to be even lower. Thus, during hot pressing, it is likely that the local stresses around particle contacts are considerably higher than the nominal applied stress and can exceed the flow stress, thereby leading to plastic flow, which can aid densification.

An additional mechanism for densification comes from vacancy creation through nonstoichiometry, which is known to enhance the mass transport through solid-state diffusion during sintering in ceramics. Nonstoichiometric carbides are characterized by a large effective diffusion coefficient (D_{eff}), as a result of which they sinter more easily than stoichiometric carbides.[33] The D_{eff} for ZrC_x phases was found to grow appreciably with the increase in carbon-vacancy concentration at all temperatures, including an increase from 5.1×10^{-15} $m^2\ s^{-1}$ for $ZrC_{0.95}$ to 1×10^{-10} $m^2\ s^{-1}$ for $ZrC_{0.68}$ at 1800 °C. It has been shown that the activation energy for grain growth for ZrC_x decreases from 53.4 kcal/mol at $x = 0.97$ to 42.8 kcal/mol at $x = 0.65$.[34]

Thus, even though ZrB_2, the primary phase in both composites, is not expected to change its densification behavior, we believe that the existence of a substoichiometric ZrC plays a major role in enabling densification at temperatures as low as ~1200 °C (Reaction [2]) due to enhanced plastic flow[35–37] and creep[38,39] in hot pressing, whereas the composite containing the stochiometric carbide requires at least 1600 °C. The final RD values of the stochiometric composites in the present work are similar to those obtained by RHP[16] at a much higher temperature of 1900 °C. Broadly speaking, it may be noted that the ZrB_2-ZrC composites produced in the present work have similar grain size to those of ZrB_2 produced at 1700 °C[18] and are significantly finer than those reported at higher temperatures.[10,11,15] The hardnesses of the composites are better than those displayed by similar materials made earlier,[11,15] presumably due to the refinement in microstructure.

The effect of Ni addition on completion of reaction and densifications can be summarized as follows. The Zr-Ni binary phase diagram[40] (Figure 11) reveals a eutectic at ~960 °C. At low processing temperatures (*e.g.*, 1000 °C for 5 minutes), Ni aids in the formation of Zr-Ni liquid phase locally, wherein the B_4C dissolves, forming ZrB_2 and ZrC phases, and with an increase in time, the local Ni concentration increases and leads to solidification. In the presence of Ni, the reaction goes to completion in stoichiometric and nonstoichiometric composites, as indicated by the absence of B_4C in the final products at 1200 °C (Figures 3(a) and 8(b)). In the nonstoichiometric mixture, however, the excess Zr present in the mixture prolongs the duration of Zr-Ni liquid, resulting in densification at lower temperature (1200 °C). However, in contrast to our earlier observation in Ti-BN,[19] densification appears to proceed

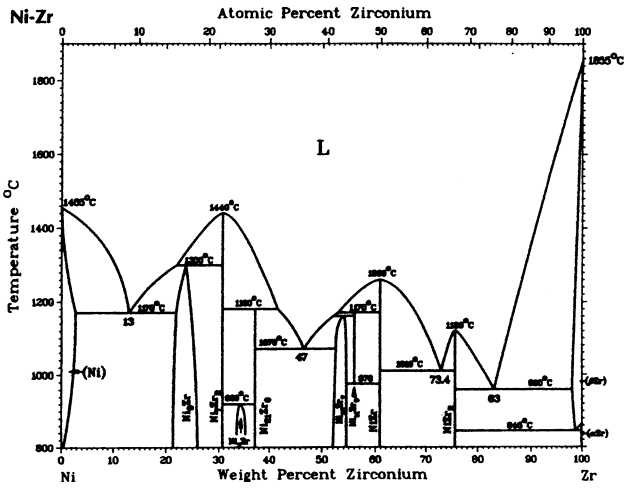

Fig. 11—Zr-Ni phase diagram[40] showing a eutectic at ~960 °C near the Zr-rich end.

somewhat independently of the reaction, and high final densities can be reached by plastic flow and diffusion in ZrC even in the presence of unreacted B_4C particles.

V. CONCLUSIONS

The present study on RHP of ZrB_2-ZrC and ZrB_2-$ZrC_{x\sim0.67}$ composites has led to the following conclusions.

1. RHP can lower the formation and densification temperature for stoichiometric ZrB_2-ZrC composites to ~1600 °C, yielding a RD of ~97 pct. This temperature can be brought down to 1200 °C using excess Zr to yield ZrB_2-ZrC_x composites with $x \sim 0.67$ and ~99 pct RD.
2. The formation of ZrB_2 and ZrC_x are well underway at 1000 °C in the nonstoichiometric mixture, while a small addition of Ni (1 wt pct) helps to ensure both reaction as well as densification at 1200 °C.
3. The grain sizes of 0.64 ± 0.3 μm for the ZrB_2 and 0.43 ± 0.2 μm for the $ZrC_{x\sim0.67}$ phases in the nonstoichiometric mixture are much finer than those seen in the stoichiometric mixtures, while both are similar to those reported elsewhere for ZrB_2 made by Zr-B hot pressing and are significantly finer than those reported for hot-pressed powders of ZrB_2 and ZrC. The rapid low-temperature (1200 °C) densification likely arises from a combination of rapid diffusion due to the microstructural refinement and plasticity in nonstoichiometric $ZrC_{x\sim0.67}$.
4. By taking advantage of all the process variables, it is possible to produce ZrB_2-$ZrC_{x\sim0.67}$ composites with a RD and hardness of 99 pct and 22.1 ± 0.7 GPa, respectively, at 1200 °C.

ACKNOWLEDGMENTS

The work that has been reported is a result of support from Director, NAL, Head, Materials Science Division, NAL, and a grant to the Indian Institute of Science from the Defence Research and Development Organization. The authors are indebted to Messrs. V. Babu and P.M. Jaman for assistance in hot pressing experiments, Dr. S. Usha Devi for XRD measurements, and Dr. G.S. Avadhani and Mr. Keshab Barai for their assistance in the SEM work.

REFERENCES

1. K. Upadhya, J.M. Yang, and W.P. Hoffman: *Am. Ceram. Soc. Bull.*, 1997, vol. 76 (12), pp. 51–56.
2. F. Monteverde, S. Guicciardi, and A. Bellosi: *Mater. Sci. Eng. A*, 2003, vol. A346 (1–2), pp. 310–19.
3. C. Mroz: *Am. Ceram. Soc. Bull.*, 1995, vol. 74 (6), pp. 164–66.
4. C.C. Sorrell, H.R. Beratan, R.C. Bradt, and V.S. Stubican: *J. Am. Ceram. Soc.*, 1984, vol. 67 (3), pp. 190–94.
5. C.C. Sorrell, V.S. Stubican, and R.C. Bradt: *J. Am. Ceram. Soc.*, 1986, vol. 69 (4), pp. 317–21.
6. W.B. Johnson, T.D. Claar, and G.H. Schiroky: *Ceram. Eng. Sci. Proc.*, 1989, vol. 10 (7–8), pp. 588–98.
7. T.D. Claar, W.B. Johnson, C.A. Andersson, and G.H. Schiroky: *Ceram. Eng. Sci. Proc.*, 1989, vol. 10 (7–8), pp. 599–609.
8. W.B. Johnson, A.S. Nagelberg, and E. Breval: *J. Am. Ceram. Soc.*, 1991, vol. 74 (9), pp. 2093–101.
9. E. Breval and W.B. Johnson: *J. Am. Ceram. Soc.*, 1992, vol. 75 (8), pp. 2139–45.
10. S.K. Woo, C.H. Kim, and E.S. Kang: *J. Mater. Sci.*, 1994, vol. 29, pp. 5309–15.
11. T. Tsuchida and S. Yamamoto: *Solid State Ionics*, 2004, vol. 172 (1–4), pp. 215–16.
12. T. Tsuchida and S. Yamamoto: *J. Euro. Ceram. Soc.*, 2004, vol. 24, pp. 45–51.
13. F. Monteverde, A. Bellosi, and S. Guicciardi: *J. Euro. Ceram. Soc.*, 2002, vol. 22, pp. 279–88.
14. S.C. Zhang, G.E. Hilmas, and W.G. Fahrenholtz: *J. Am. Ceram. Soc.*, 2006, vol. 89 (5), pp. 1550–54.
15. K.H. Kim and K.B. Shim: *Mater. Charact.*, 2003, vol. 50, pp. 31–37.
16. G.J. Zhang, M. Ando, J.F. Yang, T. Ohji, and S. Kanzaki: *J. Euro. Ceram. Soc.*, 2004, vol. 24, pp. 171–78.
17. M.W. Barsoum, A. Zavaliangos, S.R. Kalidindi, T. El-Raghy, and D. Brodkin: *JOM*, 1995, vol. 47 (11), pp. 52–55.
18. A.L. Chamberlain, W.G. Fahrenholtz, and G.E. Hilmas: *J. Am. Ceram. Soc.*, 2006, vol. 89 (12), pp. 3638–45.
19. L. Rangaraj, C. Divakar, and V. Jayaram: *J. Am. Ceram. Soc.*, 2004, vol. 87 (10), pp. 1872–78.
20. K. Wang and V.D. Kristic: *Acta Mater.*, 2003, vol. 51, pp. 1809–19.
21. E.K. Storms: *The Refractory Carbides*, Academic Press, New York, NY, 1967, vol. 2, pp. 18–34.
22. S.L. Dole, S. Prochazka, and R.H. Doremus: *J. Am. Ceram. Soc.*, 1989, vol. 72 (6), pp. 958–66.
23. S. Baik and P.F. Becher: *J. Am. Ceram. Soc.*, 1987, vol. 70 (8), pp. 527–30.
24. A.L. Chamberlain, W.G. Fahrenholtz, and G.E. Hilmas: *J. Am. Ceram. Soc.*, 2006, vol. 89 (2), pp. 450–56.
25. S. Zhu, W.G. Fahrenholtz, G.E. Hilmas, and S.C. Zhang: *J. Am. Ceram. Soc.*, 2007, vol. 90 (11), pp. 3660–63.
26. D.B. Miracle and H.A. Lipsitt: *J. Am. Ceram. Soc.*, 1983, vol. 66 (8), pp. 592–97.
27. D.J. Rowcliffe: *Plastic Deformation of Transition Metal Carbides, Deformation of Ceramics II*, Richard E. Tressler and Richard C. Bradt, eds., Plenum Publishing Corporation, New York, 1984, pp. 49–71.
28. W.S. Williams: *J. Appl. Phys.*, 1964, vol. 35 (4), pp. 1329–38.
29. L.E. Toth: *Transition Metal Carbides and Nitrides*, Academic Press, New York, NY, 1971, vol. 7, pp. 71–84.
30. D.W. Lee and J.S. Haggerty: *J. Am. Ceram. Soc.*, 1969, vol. 52 (12), pp. 641–47.
31. M.W. Barsoum and B. Houng: *J. Am. Ceram. Soc.*, 1993, vol. 76 (6), pp. 1445–51.

32. G. Wen, S.B. Li, B.S. Zhang, and Z.X. Guo: *Acta Mater.*, 2001, vol. 49, pp. 1463–70.
33. S.S. Ordanyan, A.K. Kravchik, and V.S. Neshpor: *Powder Metall. Met. Ceram.*, 1977, vol. 16 (12), pp. 57–61.
34. G.V. Samsonov and S.A. Bozhko: *Powder Metall. Met. Ceram.*, 1970, vol. 9 (3), pp. 35–38.
35. G.E. Mangsen, W.A. Lambertson, and B. Best: *J. Am. Ceram. Soc.*, 1960, vol. 43 (2), pp. 55–59.
36. A.K. Kakar and A.C.D. Chaklader: *J. Appl. Phys.*, 1967, vol. 38 (8), pp. 3223–30.
37. J.D. McClelland and E.H. Zehms: *J. Am. Ceram. Soc.*, 1963, vol. 46 (2), pp. 77–80.
38. R. Chang and C.G. Rhodes: *J. Am. Ceram. Soc.*, 1962, vol. 45 (8), pp. 379–82.
39. T. Vasilos and R.M. Spriggs: *J. Am. Ceram. Soc.*, 1963, vol. 46 (10), pp. 493–96.
40. *ASM Handbook*, vol. 3, *Alloy Phase Diagrams*, ASM INTERNATIONAL, Materials Park, OH, 1992, p. 2.322.